Journal of Energy Storage 113 (2025) 115527

Contents lists available at ScienceDirect

Journal of Energy Storage

journal homepage: www.elsevier.com/locate/est

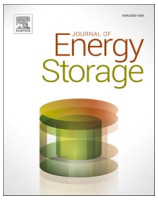

Research papers

Biochar-Ni nanocomposites derived from broccoli as an efficient ecoconscious approach for sustainable supercapacitive materials

Pablo Arévalo-Cid [a], Lorena Alcaraz [b], R.S. Sampaio [a], Felix A. López-Gómez [b], Patrícia A. Carvalho [c,d], M.F. Montemor [a], Marta M. Alves [a,*]

[a] Departamento de Engenharia Química, Centro de Química Estrutural, Institute of Molecular Sciences, Instituto Superior Técnico, Universidade de Lisboa, Av. Rovisco Pais, 1049-001 Lisboa, Portugal
[b] National Center for Metallurgical Research (CENIM), Spanish National Research Council (CSIC), Avda. Gregorio del Amo, 8, 28040 Madrid, Spain
[c] CeFEMA, Instituto Superior Técnico, Universidade de Lisboa, Av. Rovisco Pais, 1049-001 Lisboa, Portugal
[d] SINTEF Materials Physics, Forskningsveien 1, 0373 Oslo, Norway

ARTICLE INFO

Keywords:
Bionanocomposites
Broccoli
Energy storage
Hyperaccumulator
Nickel

ABSTRACT

The increasing need for energy storage systems in the transition to renewable energy is accelerating the search for sustainable raw materials, with hyperaccumulator plants offering unique, untapped sources by capturing and processing electroactive metals like nickel (Ni) into their carbon matrix. In this study, we investigated broccoli's ability to absorb and process Ni, a metal that significantly contributes to enhanced energy storage capacity. Unlike traditional phytoremediation, we focused on producing carbon-based materials with electrochemical performance rather than environmental recovery. To demonstrate our ecoconscious concept, broccoli plants were exposed to varying Ni concentrations (0, 0.4, 0.8, 1.6, and 3.2 g/L) over 10 weeks, producing shoot dry biomass with Ni contents from <20 to 492 mg Ni/kg. Following pyrolysis at 650 °C, the resulting biochar was used as electroactive material for supercapacitor applications. Surprisingly, the best performance was observed in plants with 152 mg Ni/kg, with the bionanocomposite exhibiting a specific capacitance of 38 F/g at the scan rate of 100 mV/s and excellent capacitance retention of 94 % over 5000 cycles at 10 A/g. The supercapacitor prototype presented a maximum energy density of 0.762 Wh/kg at 184 W/kg power density. This unexpected finding suggests altered plant metabolism as a potential explanation, offering new insights and raising scientific questions about engineering hyperaccumulator plants for sustainable energy storage applications.

1. Introduction

Nickel (Ni) is one of the most common trace metals discharged into the environment by natural and anthropogenic activities. Natural processes (rock erosion, weathering, and volcanic eruptions), industrial activities (industry effluents, mining activities, electroplating, batteries, and paint industries), various agricultural products (fertilisers and pesticides), and urban sources (municipal sewage sludge and landfills) are primary sources of Ni contamination in terrestrial ecosystems [1,2]. Both natural and anthropogenic sources contribute to Ni enrichment in soils. However, bioavailability is much lower in naturally enriched soils compared to those contaminated by human activities, even when total Ni levels are similar [3]. Soils contaminated with Ni have been reported to contain concentrations ranging from 0.2 to 450 mg/kg [4]. In contaminated soils, Ni is adsorbed onto clays, oxides, hydroxides, or humic substances. The nature and strength of this bonding are influenced by soil physicochemical properties, thereby governing the release of Ni from contaminated soil surfaces into the soil solution and its subsequent bioavailability [5].

While Ni contamination in soils has detrimental effects on the biosphere, some Ni species offer high conductivity and potential for electrochemical energy storage and have been intensively studied for batteries and supercapacitors [6]. Ni oxides and hydroxides can exhibit reversible electrochemical capacity even when charged at a high cut-off voltage in various battery applications when used as a redox centre. The distinct oxidation states of Ni^{2+} and Ni^{3+} can be attained in common cathode materials, while higher specific capacity is achievable using the Ni^{2+}/Ni^{4+} redox couple [6]. Integrating Ni-based compounds with carbon materials to boost electronic conductivity and design carbon structures featuring porous, hollow, and hierarchical properties is the

* Corresponding author at: Instituto Superior Técnico, Av. Rovisco Pais, 1049-001 Lisboa, Portugal.
E-mail address: martamalves@tecnico.ulisboa.pt (M.M. Alves).

https://doi.org/10.1016/j.est.2025.115527
Received 15 July 2024; Received in revised form 14 October 2024; Accepted 23 January 2025
Available online 31 January 2025

most effective approach for achieving exceptional properties in electrochemical energy storage [6].

This critical role of Ni in enhancing the performance of batteries and supercapacitors is essential for supporting the transition from fossil fuels to renewable energies, establishing Ni as a fundamental raw material in this sector [6,7]. High-power energy storage devices are vital in capturing and storing excess energy produced by intermittent sources for later use. Hence the sustainability of electroactive material sources is crucial in facilitating the transition to cleaner energy. However, current technologies fall short of meeting sustainability and CO_2 footprint criteria because the active electrode materials are primarily sourced through energy-intensive mining processes [8,9]. Also, given the growing demand for Ni and its high price, there is high pressure on developing energy storage systems based on green, sustainable, and economically affordable materials. Sustainable solutions for Ni extraction can emerge from soil clearance through phytoremediation processes, a gap we aim to explore.

Among the different processes (soil washing, electro-remediation, vitrification, etc.), phytoremediation is one of the most sustainable, eco-friendly, and economical approaches for remediating Ni-contaminated soil [2]. Plants uptake bioavailable Ni through passive diffusion (utilising the cation transport system) and actively transport chelated Ni compounds (using transport proteins like permeases) [5]. The ratio of active and passive uptake of Ni depends on the plant species, presence of organic matter, the ionic form of Ni, pH of growth media, and Ni and other ions contents in soil [10]. Once inside the plant, Ni is transported via the xylem (from roots to shoots and leaves) through the transpiration stream. In contrast, in the phloem (towards buds, fruits, and seeds), Ni transportation is regulated by metal-ligand complexes (e.g. histidine, nicotinamide, organic acids, and specific Ni binding proteins) [5]. A higher value of Ni translocation from root to shoot has been pinpointed as one of the factors responsible for higher growth under Ni toxicity [11]. To prevent the disruption of essential cellular processes (e.g., photosynthesis), once in the plants, Ni is primarily stored in epidermal cells and cell vacuoles through iron-regulated/ferroportin (IREG/FPN) transporters or by chelation with N- and S- rich ligands [4,10,12]. Cell walls may also contribute to metal detoxification depending on the plant species, with the apoplast cell walls potentially containing 60–70 % of accumulated Ni [10]. The compartmentalisation of hyperaccumulated Ni and their possible cell wall connections are still controversial [10]. While Ni is necessary for improving plant development and growth (0.05–10 mg/kg dry weight) it can reach values >50 mg/kg dry weight in tolerant species [10].

Ni plays varied roles in energy storage devices. Pure Ni compounds are renowned in batteries for their stable performance and capacity over numerous cycles [13]. For supercapacitors, incorporating Ni into biochar derived from plant material is expected to enhance conductivity, redox reactivity, surface area, and overall stability, similar to improvements observed in other metal-containing carbon matrices [14–17]. This is expected to result in a significantly improved electrochemical performance compared to biochars without Ni loading.

Our work explores using this novel ecoconscious electroactive material concept for supercapacitors. Biomass-derived carbon materials have been extensively researched as efficient electrode candidates due to their well-developed tailored textures (closed pores and defects) and large microcrystalline interlayer. The carbonisation of plant biomass makes it possible to produce environmentally friendly materials with the desired properties [18]. While traditionally, phytoremediation has not focused on final metrics [19,20], the challenge lies in defining the uptake conditions that yield optimal electrochemical performance.

In this paper, we investigate the electrochemical performance of Ni-contaminated biochar derived from broccoli, a Ni-hyperaccumulator plant [21–23] cultivated in soils with varying cumulative Ni concentrations, to demonstrate its potential for electrode development.

2. Materials and methods

2.1. Reagents

Nickel solutions used for plant watering were formulated using nickel nitrate hexahydrate [$Ni(NO_3)_2$]. In preparing the active material-based ink, both polyvinylidene difluoride (PVDF) and *N*-methyl-2-pyrrolidone (NMP) were used as received. All reagents are from Sigma-Aldrich. The electrochemical characterisation was performed using sodium sulphate (Na_2SO_4) from Carl Roth. KOH 85 % pellets (Panreac Chemicals, Barcelona, Spain) were ground and subsequently used to prepare carbon-activated samples.

2.2. Plant and soil material

Broccoli (*Brassica oleracea* var. *italica*) seedlings, each with four leaves, were bought from a local plant supplier (Viplant, Portugal). These seedlings grown in cuvettes were transplanted into individual pots with a diameter of 12 cm, utilising a universal substrate, and irrigated with tap water. After 10 days, plants underwent a watering regimen twice a week, receiving solutions with varying nickel concentrations (Ni) - 0, 0.4, 0.8, 1.6, and 3.2 g/L, and grown outside to simulate 'field' conditions (Portugal, Lisbon). For a cumulative exposure to nickel (Ni), each plant received irrigation with 10 mL of solution for 3 weeks. Over the subsequent 6 weeks, as plant weight increased, the irrigation volume per plant for each solution was increased to 30 mL. By the 10th week, soil and shoots were collected and dried in an oven (Memmert) at 50 °C for several days until a steady dry weight was achieved. Experiments were made in duplicate. Whenever necessary, a universal insecticide (containing 0.2 % *w*/w tetramethrin and 0.1 % w/w 1R-trans-phenothrin) was applied for pest control, ensuring its usage remained below phytotoxicity thresholds.

2.3. Determination of Ni in plant biomass and soils

For the determination of Ni content, inductively coupled plasma optical emission spectroscopy (ICP-OES) analysis was used with 150 mg of dried aerial parts or substrates that were digested with 4 mL of nitric acid and 1 mL of hydrochloric acid (both from Sigma-Aldrich) in a microwave system (Ethos Touch control, Milestone Inc.). Ni content was determined with an Optima 2000DV spectrophotometer (Perkin Elmer).

2.4. Preparation of Ni-doped biochar

A methodology was proposed for the obtention of plant-derived biochar. Initially, a pyrolytic treatment was approached. For this purpose, the dry plant was powdered and placed in a ceramic crucible. It was treated in a Carbolite STF 15 tubular furnace with an N_2 flow rate of 150 mL/min to act as a gas carrier during the heating ramp (10 °C/min) up to 650 °C and maintained for 2 h. Once finished, the reactor cold down slowly to room temperature. Carbon activation with KOH was achieved by mixing the powdered precursor with KOH in a 1:2 ratio before the heat treatment in an alumina crucible. The obtained solid was washed using MilliQ water until a neutral pH was reached.

2.5. Physicochemical characterisation

For the analysis of biochar, the specific surface areas were calculated from N_2 physisorption isotherms by the Brunauer-Emmett-Teller (BET) method, and the pore size distribution (PSD) was calculated from the desorption branch of the isotherm using the Barrett-Joyner-Halenda (BJH) approach. Also, scanning electron microscopy (SEM), Scanning Transmission Electron Microscopy (STEM), X-ray diffraction (XRD) and both elemental point analysis and mapping were performed with energy-dispersive X-ray spectroscopy (EDS). A detailed description is provided in SI.

2.6. Electrochemical characterisation

SI describes detailed electrochemical responses of electrodes, accessed by cyclic voltammetry (CV), electrochemical impedance spectroscopy (EIS), and galvanostatic charge-discharge (GCD).

3. Results and discussion

3.1. Simulated plant phytoremediation

To simulate contaminated soils, where plants are exposed to cumulative amounts of nickel (Ni) from the surrounding environment, broccolis were consistently watered over time with the same nickel solution, i.e. 0, 0.4, 0.8, 1.6, and 3.2 g Ni/L. Treatments involving Ni correspond to cumulative concentrations of 0 (A), 0.1 (B), 0.3 (C), 0.6 (D), and 1.2 (E) g of Ni per 9 weeks (Fig. 1 **a**). Effectively, these treatments resulted in soil contaminations of 0.5 g Ni for treatments A and B, showing that residual Ni contents are typically present in soils. This result agrees with Ni being recognised as a natural component of soils [24]. Treatment C resulted in 1.2 g Ni. Treatment D, with 5.5 g Ni, has 10× more Ni than treatment B, and approximately half the amount is found in treatment E (10.2 g Ni) (Fig. 1 **b**). Statistically, differences in Ni content in soils are depicted between conditions D and C and A or B. These values fall within the lower range of Ni content in soils, as concentrations can vary widely, ranging from 3 to 1000 mg/kg in heavily contaminated soils [24].

After uptake, Ni is distributed throughout the aerial parts of plants and finally accumulates within the cellular structures. Ni is reported to translocate readily into the stellar tissue, facilitating its movement to the aerial parts of plants [23,25,26]. Therefore, the cumulative impact of Ni content in soils on broccoli, a known hyperaccumulator plant [21], was assessed by evaluating the effect on broccoli shoot morphology, accumulated Ni, and fresh and dry mass (Fig. 2).

No morphological differences were detected in the plants during the first 3 weeks of Ni uptake. Upon an increased volume of watering solution, the first yellowish leaves appeared 2 weeks later (data not shown). After 10 weeks (Fig. 1a), A-C treated plants exhibited typical dark green leaves, with some older leaves appearing dried. D-treated plants showed slightly smaller leaves, while *E*-treated plants displayed compromised growth, including decreased size and smaller, damaged young leaves. Still, quite a ticker young stem (Fig. 2a). Comparing the Ni content in soils (Fig. 1b) with that in shoots, statistically significant differences were observed only in treatment E, with 492 mg Ni per fresh weight. While other treatments showed no statistically significant differences, there was a clear increasing trend from around 20 mg Ni per fresh weight (A and B), 48 mg Ni per fresh weight (C), to 152 mg Ni per fresh weight (D) (Fig. 2b). In terms of fresh and dry weight. However, there was a decreasing trend with increasing Ni content; no statistically significant differences were depicted (Fig. 2c, d). This observation may be attributed to the decrease in leaf size being offset by an increase in stem thickness, which is particularly noticeable in treatment E (Fig. 2a). Similarly, an average water content of approximately 81 % was observed for all studied plants.

We observed reduced growth and leaf sizes in agreement with other brassica varieties exposed to Ni. Conversely to our findings, altered water contents were reported for cabbage (*Brassica oleracea* var. *capitata*) [27]. These morphological effects may be attributed to disrupted metabolic pathways. While Ni is an essential element for plants, excess amounts can lead to toxicity symptoms. Responses to toxicity vary significantly depending on factors such as plant species, growth stage, cultivation conditions, Ni concentration, and exposure time. Critical responses generally occur due to disruptions in photosynthesis, interference with other essential metal ions, and induction of oxidative stress [21,28].

Nickel damages the photosynthetic apparatus at nearly every level of its organisation, from destroying mesophyll and epidermal tissue cells to leading to disturbances in carbon metabolism [28]. The chemical similarity of Ni to Ca, Mg, Mn, Fe, Cu, and Zn allows Ni to compete with these metals in absorption and transpiration processes. Consequently, at high concentrations, Ni toxicity may partially result from disrupting the absorption of these essential metal ions [28], many of which have relevant electrochemical performance [29]. While some reports indicate deficiencies in these metals, others highlight increased Fe and Mn concentrations in Ni-rich soils, illustrating the complexity of plant systems adapting to elevated Ni concentrations [30]. Also, Ni acts as a cofactor for urease, an enzyme crucial for N metabolism. Urease plays a primary role in N assimilation, as it becomes accessible for plant assimilation only after hydrolysis for ammonia and carbon dioxide. N metabolism, associated with photosynthetic carbon absorption, is critical in plant development [31]. Another aspect of Ni toxicity is the heightened production of reactive oxygen species (ROS). This has been associated with lipid peroxidation, destabilised membranes, disrupted activities of membrane-bound enzymes, and ultimately altered plant carbon structure [25,32,33]. Biochar derived from close Ni concentrations (B, C and D) was analysed to evaluate the impact of Ni stress on the structural properties of the carbon matrix. Fig. 3 summarises the data obtained from the BET analysis of the N_2 adsorption isotherms for samples with Ni concentrations of 0.4 (B), 0.8 (C), and 1.6 (D) g Ni/L. As observed, the higher the Ni content, the higher the specific surface area. An increase in the surface area in the presence of Ni was also described by Yang et al. [34]. The area's rise is led by the increasing porosity found when analysing the total pore volume (V_T). This effect is remarkable considering that the pore size (as pore diameter, d_p) decreases with the Ni content, leading to a material that is close to the value established for microporosity ($\leq$ 2 nm). The reduction in pore size has been attributed previously [35] to the interaction of the Ni salts with their carbon environment during the pyrolytic process.

The physicochemical properties of shoot-derived biochar of plants collected from soils loaded with Ni with statistically significant

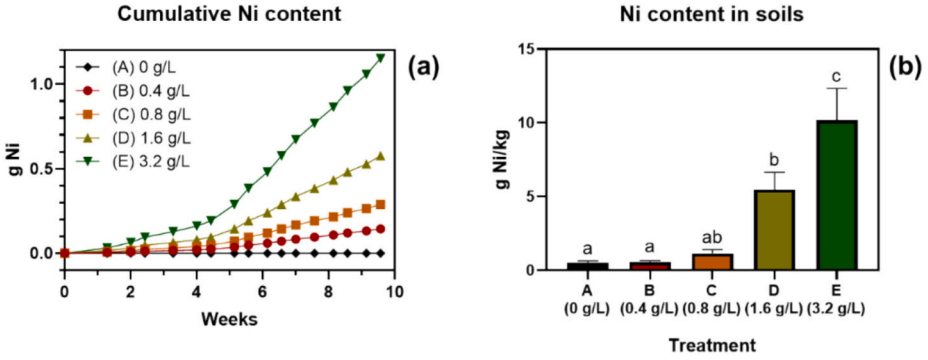

Fig. 1. Ni content in soils after watering with solutions containing 0 (A), 0.4 (B), 0.8 (C), 1.6 (D), and 3.2 (E) g Ni/L for 9 weeks; (a) calculated cumulative Ni content and (b) Ni content determined by ICP-OES. Data are presented as mean ± %CV. Statistically significant differences are denoted by distinct letters at $p \leq 0.05$.

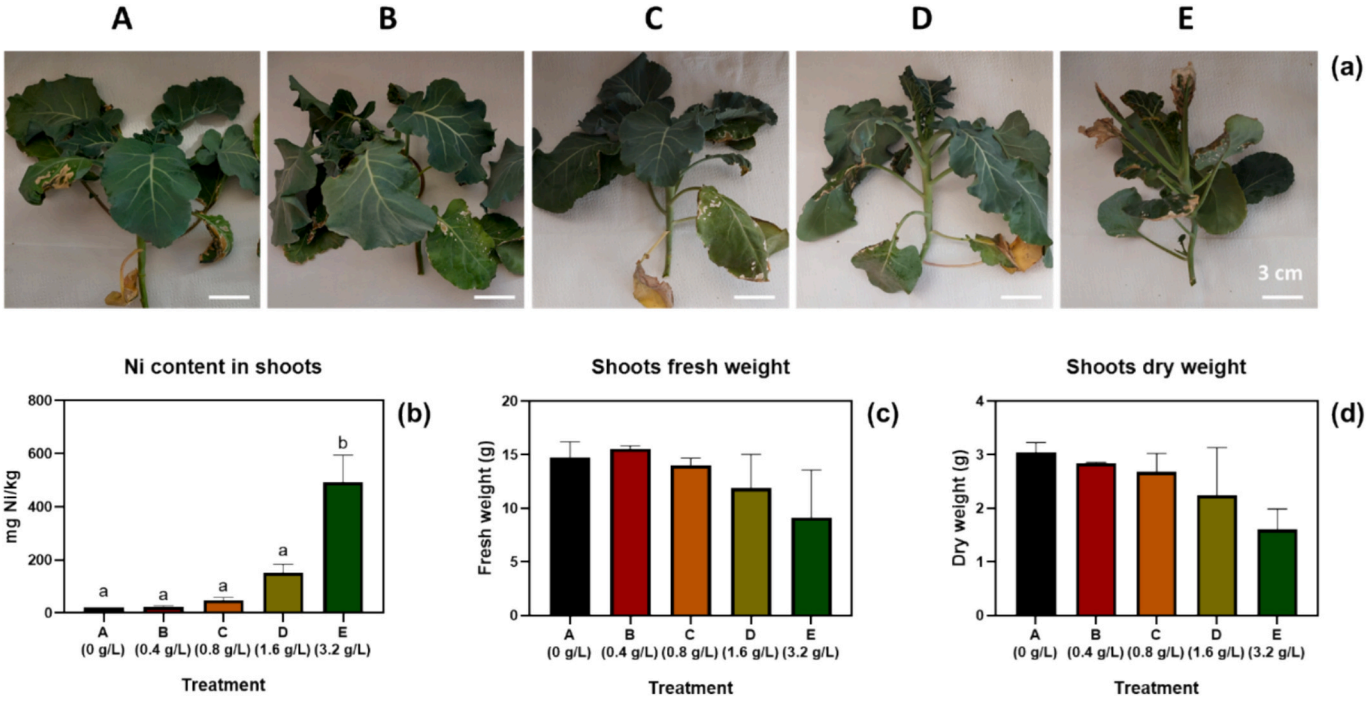

Fig. 2. Effect of Ni soil content in broccoli shoots watered with Ni-containing solution: 0 (A), 0.4 (B), 0.8 (C), 1.6 (D), and 3.2 (E) g Ni/L for 9 weeks; (a) micrographs, (b) Ni content obtained by ICP-OES, (c) fresh weight and (d) dry weight. Data are presented as mean ± %CV for Ni content and SE for weight. Statistically significant differences are denoted by distinct letters at $p \leq 0.05$.

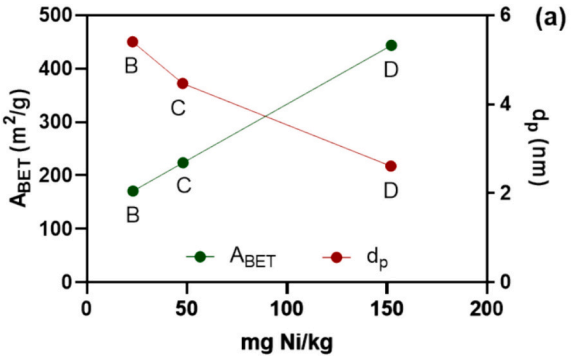

(b)

Sample	A_{BET} (m^2/g)	V_T (cm^3/g)	d_p (nm)
B (0.4 g Ni/L)	171.17	0.231	5.40
C (0.8 g Ni/L)	223.92	0.250	4.47
D (1.6 g Ni/L)	443.58	0.289	2.61

Fig. 3. Structural properties of the prepared Ni-loaded biochar (a) graphical representation of surface area (A_{BET}) and pore size (d_p) according to Ni concentration in the biochar, based on the data reported for each plant biochar.

differences in the Ni content, i.e. A, D and E (Fig. 1b) were analysed by SEM (**Fig. S2**), HR-TEM and XRD (Fig. 4).

SEM images show shoot-derived biochar structures with a porous microstructure (**Fig. S2**). The resulting morphology results from the organisation of the lignocellulosic vessel tissue, as is usual in prepared plant-derived biochars [36,37]. The detailed analyses of biochar, made by HR-TEM, showed a uniform distribution of C and O in conditions A, D, and E (Fig. 4a). While S was residual in the biochar of A, localised distribution was seen in D. Homogeneous distribution was depicted in E (Fig. 4a). This element has been associated with detoxification mechanisms used by hyperaccumulator plants to cope with high Ni contents. Most metal ions are bound to ligands and proteins with a low molecular mass, with only a tiny fraction of metals present as free ions. To do so, plants produce several metal ligands, many of which are thiols, including glutathione, phytochelatins, and metallothioneins [38]. Increased glutathione content was reported in some Ni hyperaccumulators, suggesting a potential mechanism for protection against Ni-induced oxidative damage in these plants [39]. Also, heightened activity of the S assimilatory pathway enzyme, specifically mitochondrial serine acetyltransferase, was found to be correlated with enhanced glutathione synthesis [39].

Among the main cations detected in hyperaccumulator plants, K was the major, followed by Ni, Ca, Mg, and Fe [40]. These were also the main elements identified by EDS in broccoli biochar (**Fig. S3**). A clear correlation emerged between Ni levels in the biochar and K or Mg contents (Fig. 4a), which mirrors the previously established relationship between heightened Ni and K or Mg concentrations in hyperaccumulators [26,41,42]. Reports suggest that the elevated osmolarity within the vascular system of hyperaccumulators, characterised by exceptionally high Ni concentrations in the phloem, may impact various physiological processes such as respiration and stomatal function. Consequently, this could affect K uptake and plant regulation [26,41]. Likewise, positive correlations were identified between Ni and Ca in plants [26,41]. Since leaves often harbour calcium oxalate crystals, which have an affinity for both Ca and Ni, oxalate may function as a regulatory molecule influencing the accumulation of these elements. Also, it has been suggested that the formation of crystals containing metal inclusions and their storage in vacuoles could serve as a potential mechanism to mitigate the

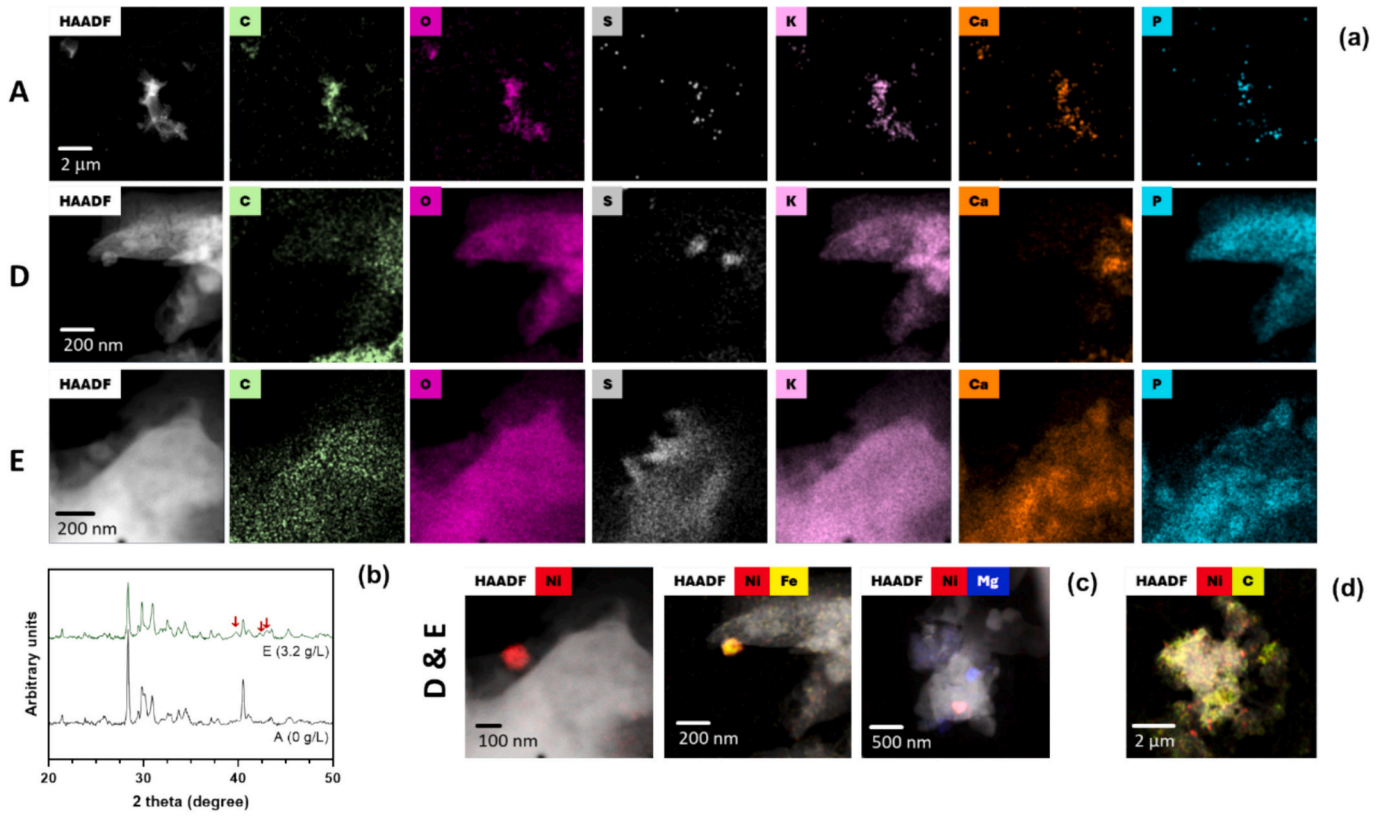

Fig. 4. Physicochemical characterisation of biochar derived from plants grown with Ni A (0 g/L), D (1.6 g/L) and E (3.2 g/L); HR-TEM images and EDS maps of (a) biochar and elemental maps of C, O, S, Ca, P and K, (b) Ni-based nanoparticles distributed in the biochar identified by Ni and C elemental distribution, (c) Ni-based nanoparticles composition identified elemental distribution of Ni, Fe and Mg, (d) XRD pattern of the biochar.

toxic effects of metals in plants [26].

The distribution of P closely mirrored that of O (Fig. 4a), indicating a preference for phosphate formation in plants cultivated in the presence of Ni (D and E). Conversely, residual P contents coincident with O mapping in plants grown without Ni (A) suggest minimal phosphate formation (Fig. 4a). These observations collectively support that Ni(II)-phosphate complexes may also be forming. The absence of O in EDS mapping (Fig. 4a *row E*) suggests the formation of metallic Ni nanoparticles with sizes around 100 nm (Fig. 4). The XRD patterns in Fig. 4b display typical peaks of plant-derived biochar [43] alongside a new peak observed in E around 43°, corresponding to metallic Ni formation, as evidenced by its diffraction maximum at this 2θ value [44]. This is further corroborated in Fig. 4a, c, where no direct correlation between the amount of Ni and O exists, denying the presence of Ni oxides. High levels of C naturally found in plant biomass may contribute to the formation of Ni carbides, providing a potential explanation for peaks at 39° and 42° (Fig. 4b). In plants, various carbon sources contribute to the composition of biochar, with components such as the cell wall matrix being notably persistent. For instance, studies demonstrating that cell walls can accumulate high concentrations of Ni [45] further support our assumption. The presence of Fe (Fig. 4c) and diffraction maxima for metallic iron (α-Fe) found at around 44° angle values (Fig. 4b) [46] suggests as well the formation of metallic nanoparticles. The preferred formation of Ni and Fe metallic phases instead of their oxide counterparts during the preparation of activated carbon nanocomposites under an inert atmosphere has been previously observed, independently of the nature of the carbon source (biological [47] or synthetic [48]). The reducing character of carbon has been proposed as the cause of obtaining metal particles instead of their oxides. While the formation of metallic Ni nanoparticles has been ascribed, its distribution across the biochar matrix has been analysed by examining the Ni distribution over C, revealing a relatively uniform dispersion of Ni within the carbon matrix (Fig. 4d).

Electrodes made solely of pure carbon are commercially used in supercapacitors and rely on the electrochemical double-layer mechanism for charge storage. Usually, these devices exhibit modest energy density, thus limiting their possible range of applications. Incorporating Ni and Fe within commonly used carbon-based materials can provide abundant active sites and additional conductivity, thereby enhancing the electrochemical performance of these materials [14,15]. Metallic Ni and Fe have garnered significant interest as electrode materials by enhancing electron transport and boosting charge storage capacity [14–16]. As an example, in Ni:C nanocomposites with metallic Ni content of 12 wt%, reversible capacities of 728 and 541 mAh/g at the first and 50th cycles were reported, corresponding to a capacity retention of 75 % at the current density of 50 mA/g [49]; for core-shell structured C–metallic Fe anodes were reported to offer high electrochemical activity and stability, achieving a specific capacity of 208 mA/g at a current density of 1 A/g, and capacity retention of 93 % after 2000 cycles at 4 A/g [15]. Also, hierarchically activated porous carbon from Mg-based metal-organic frameworks (MOF) was reported with a high specific capacitance of 362.5 F/g at 1 A/g and excellent cyclic durability with 94.2 % capacitance retention over 150,000 cycles at 50 A/g [16].

Hence, evaluating the electrochemical performance of broccoli biochar becomes crucial. This allows for assessing the contributions of elements such as Ni, Fe, and Mg, along with potential C matrix alterations, thereby defining their suitability for energy storage applications.

3.2. *Contaminated biomass for tunned supercapacitor application*

Traditional synthetic systems offer controlled component amounts in nanocomposites. Still, plant-derived biochar usage hinges on toxicity from the target element, like Ni, and metabolic impacts on other electroactive element uptake. Thus, electrodes derived from conditions A-E

underwent electrochemical performance testing.

The electrochemical response of all materials was evaluated through GCD and CV at different specific currents and scan rates, respectively, in a 1 M Na_2SO_4 aqueous solution. The active mass of the modified electrodes was approximately 1 mg. The optimum working potential window was between −100 and 650 mV vs. SCE. The specific capacitance, C_s, was determined from the GCD transients according to the equation:

$$Cs = \frac{i.t_d}{m.\Delta E}$$

Where t_d is the discharge time, i is the applied current, m is the active material mass, and ΔE is the working potential window. A detailed electrochemical characterisation of the sample without Ni is represented in **Fig. S4**. The cyclic voltammograms at lower (from 5 to 100 mV/s) and higher scan rates (from 100 to 500 mV/s), shown in **Fig. S4 a** and **b**, present an almost rectangular shape, even at high scan rates, which is characteristic of a capacitive response with high reversibility during the charge-discharge process. The GCD curves at different specific currents (from 0.5 to 10 A/g) present a triangular profile (**Fig. S4 c**) with Coulombic efficiency close to 100 % (**Fig. S4 e**) and low ohmic drop (from 3.4 to 68.1 mV). The specific capacitance as a function of the applied current is represented in **Fig. S4 d**. The electrode exhibited a specific capacitance of 40 F/g at 1 A/g and a good capacitance retention of about 82 % at 10 A/g. The capacitive behaviour is also visible in the impedance spectrum at lower frequencies, where the evolution of the Nyquist data points is almost vertical (**Fig. S4 f**). At high frequencies, the impedance spectrum presents a depressed semi-circle. These features are characteristic of a carbon material without any redox features. The equivalent electric circuit used for the numerical fitting of impedance spectra (**Fig. S5a**) was based on literature [50]. The model is constituted by the resistance of the electrolyte (R_S), the distribution of charge in the frequency domain (CPE_1), charge transfer resistance (R_{CT}), Warburg impedance (W), double layer capacitance (CPE_S), and self-discharge resistance (R_{SD}). The electrolyte and charge transfer resistances were

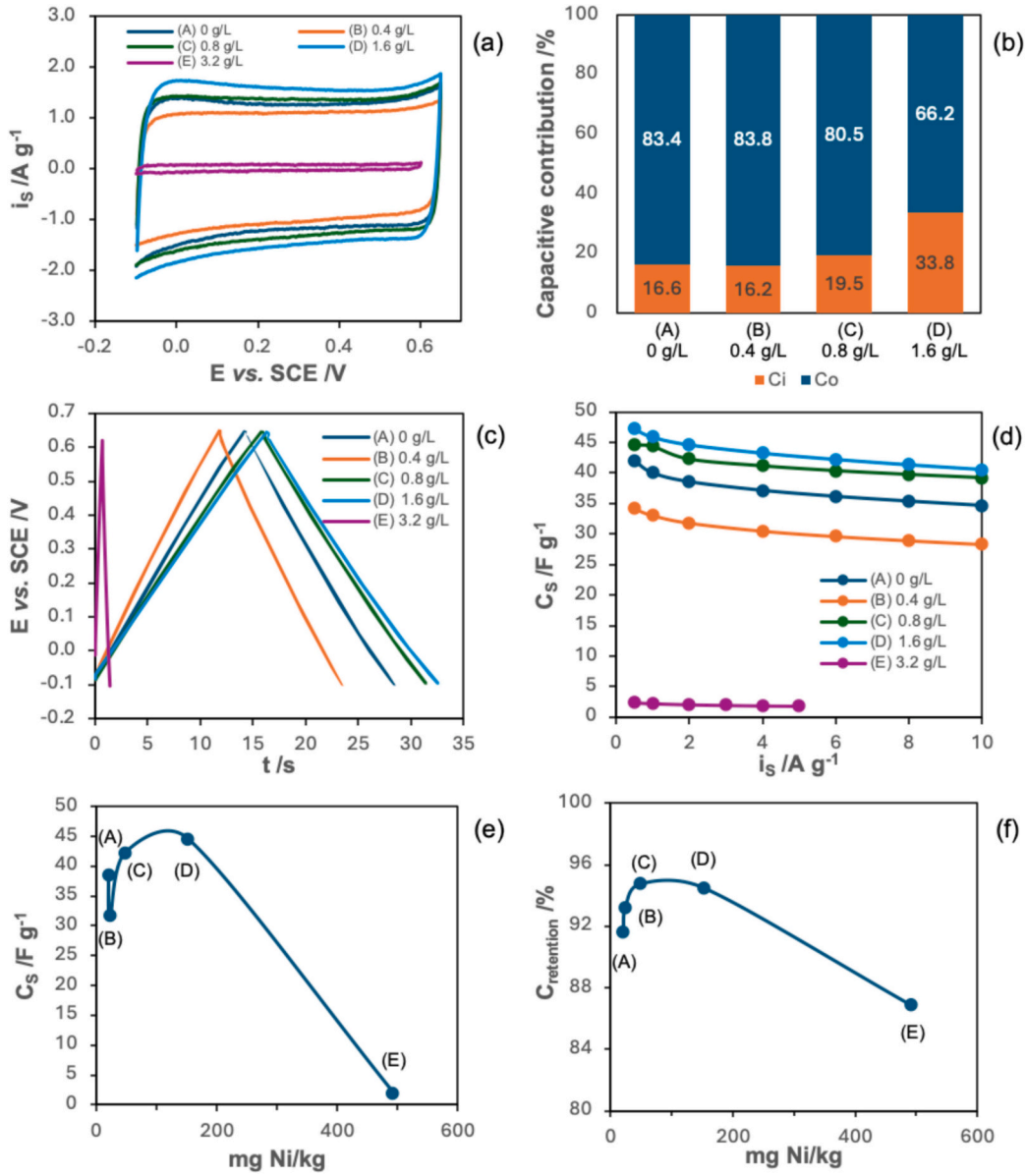

Fig. 5. Electrochemical characterisation of electrodes composed of carbon with different Ni content: (a) Cyclic voltammograms at 40 mV/s, and (b) Percentage of capacitance contribution evaluated for all modified electrodes based on Trasatti analysis (Ci and Co are the inner and outer surface charge contributions, respectively); (c) GCD at 2 A/g; (d) Specific capacitance as a function of the applied current; (e) Specific capacitance and (f) Capacitance retention at 2 A/g as a function of Ni content.

4.2 and 0.29 Ω cm^2, respectively. The specific capacitance estimated according to the Brug equation [51] was 41.1 F/g, similar to the value obtained by GCD at 1 A/g (40 F/g).

The electrochemical characterisation of electrodes composed of carbon with different Ni content is summarised in Fig. 5. The cyclic voltammograms at 40 mV/s and GCD profiles at 2 A/g of the other samples present a similar shape (**Fig. 5a** and **c**), which is indicative of a similar charge mechanism. The absence of redox peaks corroborates the presence of metallic nanoparticles in the carbon matrix (Fig. 4). The specific capacitance and the capacitance retention as a function of the applied current of all samples are represented in **Fig. 5d** and **e**, respectively. The capacitance, despite decreasing slightly in B, shows an increase in samples C and D compared to the sample without Ni (A) (Fig. 5e). The biochar of Ni-watered plants (B-E) shows increased capacitance retention at higher specific currents (Fig. 5f). The presence of Ni (and possibly Fe and Mg) can lead on one hand to enhanced electron transport and charge storage capacity of carbons [14–16] and on another hand to the formation of more porous materials due to the easiest depolymerisation of lignocellulosic components within the biomass during the thermal treatment and to increased bond cleaving [17]. The electrochemical performance of these samples is well comparable with the metrics of other biochar-based materials without functionalisation. Biochars from dairy manure and sewage sludge, loaded with Ni and without additional treatment, showed a specific capacitance, at 5 mV/s, of 39.1 and 33.2 F/g, respectively [52], while sample D (1.6 g Ni/L) exhibited a specific capacitance of c.a. 38 F/g at a high scan rate of 100 mV/s. Further comparisons with reported Ni-based electroactive materials for supercapacitor applications can be found in **Table S1**. Generally, biochar materials are still far from demonstrating specific capacitances comparable to Ni-MOF structures, underscoring the urgent need to enhance the electrochemical performance of these ecoconscious materials.

The capacitive contribution of the modified electrodes was further evaluated using Trasatti's method [53]. According to this analysis, the total charge stored comprises an inner and an outer surface charge. The inner contribution is less accessible and controlled by diffusion, while the outer is more accessible and non-diffusion controlled. As expected for a carbon-based material, the capacitance is mainly governed by the electrical double-layer contribution, which is expressed in the higher outer surface charge, as can be seen in Fig. 5b. The increase in the amount of Ni led to a rise in inner surface charge contribution, which aligns with increased porosity (Fig. 3), presenting a similar evolution to that of the specific capacitance as a function of the Ni amount (Fig. 5e).

The electrical parameters of impedance spectra (specific capacitance, solution, charge transfer and self-discharge resistances) of each modified electrode were estimated from the EIS fitting and are represented in **Fig. S5**. The variation of capacitance as a function of Ni content, shown in **Fig. S5b**, agrees with the results obtained by the GCD transients (Fig. 5e) and the estimated metrics. The electrolyte resistance is almost constant for all modified electrodes. The charge transfer resistance slightly increased with the increasing Ni load, while the self-discharge resistance decreased substantially. The self-discharge phenomenon was confirmed by open circuit potential evaluation for 30 min after a galvanostatic charge of electrodes at 1 A/g — the electrodes with lower Ni discharge faster, corroborating the impedance results.

The long-cycling stability of the modified electrodes was determined by GCD test for 5000 cycles at 10 A/g, as can be seen in Fig. 6. The electrodes present an excellent capacitance retention of about 94 % (Fig. 6a), maintaining a Coulombic efficiency nearly 100 % (Fig. 6b), and with an increase in the ohmic drop lower than 2 mV (Fig. 6c). The long-cycling test did not significantly affect the performance of the electrodes, which after 5000 cycles did not change noticeably in the shape of the GCD profile (Fig. 6c). Nyquist plots, before and after long cycling, are almost coincident at higher frequencies (Fig. 6d **inset**) and only present a slight increase in the imaginary part of the impedance at low frequencies after the stability test, which indicates a decrease in the

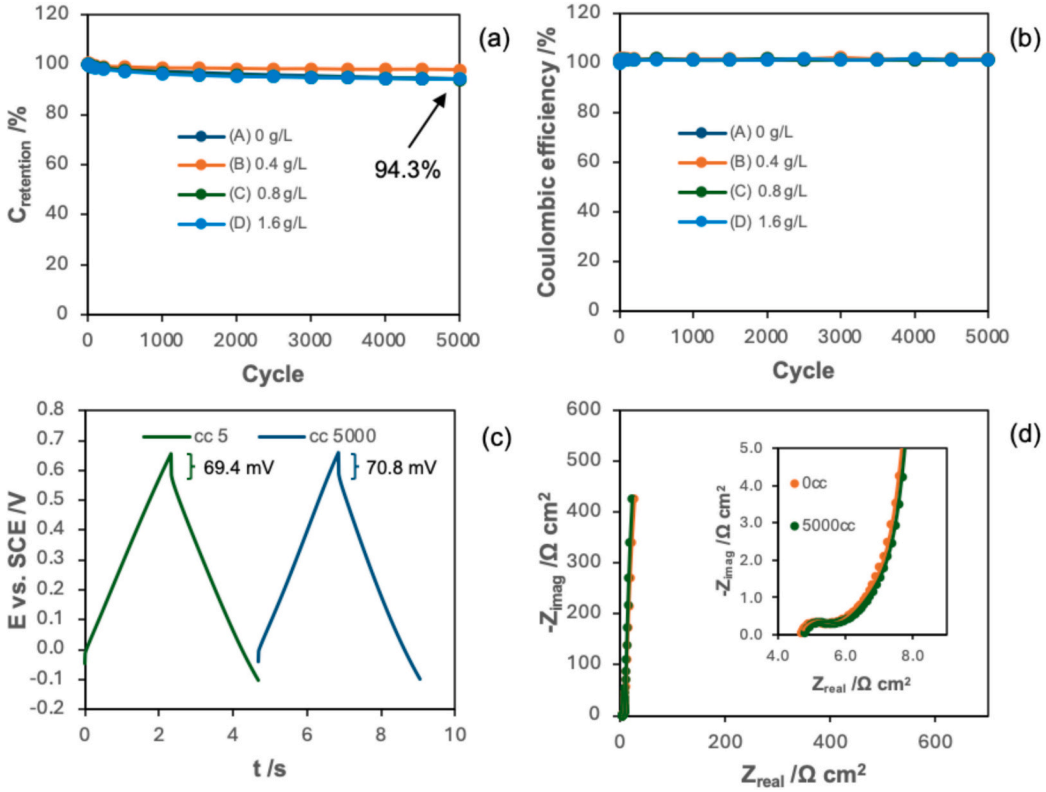

Fig. 6. Extended cycling characterisation of all samples for 5000 GCD cycles at 10 A/g: (a) Capacitance retention, (b) Coulombic efficiency, (c) 5th and 5000th GCD cycles from sample D, and (d) Nyquist plots before and after 5000 GCD cycles at 10 A/g from sample D (dots – experimental data; line – fitted data).

electrode capacitance ($Z'' = \frac{1}{jw\,C}$) (Fig. 6d). The solution resistance was 4.7 Ω cm^2, and the charge transfer resistance was 0.911 and 0.915 Ω cm^2, before and after 5000 GCD cycles, respectively.

Finally, the modified electrodes that exhibited the best electrochemical performance (sample D, 1.6 g Ni/L), namely the highest specific capacitance, were used to assemble a symmetric cell and test the performance of a supercapacitor prototype. The active mass of each electrode was 1 mg. The electrochemical response of the device was evaluated by GCD and CV in 1 M Na_2SO_4 with a working potential window of 750 mV, as obtained for the 3-electrode configuration. The specific capacitance was calculated using eq. 1 but considering the total active mass of both electrodes (2 mg). The energy and power density were calculated according to the following equations respectively:

$$E = \frac{1}{2} C_{cell} V^2$$

$$P = \frac{E}{t_d}$$

E is the gravimetric energy density, C_{cell} is the cell capacitance, V is the voltage window, and t_d is the discharge time. Fig. 7 presents the electrochemical performance of the device. The potentiodynamic characterisation of the cell is represented in Fig. 7a. The device maintained the high reversibility that was exhibited by the modified electrode in a 3-electrode configuration, as shown in the almost rectangular shape of the cyclic voltammograms, even at high scan rates, such as 500 mV/s. The GCD curves obtained at different applied currents (0.5, 1, 2, 3, 4 and 5 A/g) (Fig. 7b) present a triangular shape, as expected for a carbon-based supercapacitor. The variation of the specific capacitance as a function of the applied current is shown in Fig. 7c. The device presented a specific capacitance of 9.88 F/g, which is about 4 times lower than the single electrode capacitance, and exhibited good capacitance retention of 89 %, at 5 A/g, corroborating the high reversibility of the cell evidenced by the cyclic voltammograms. The maximum energy density of the device was 0.762 Wh/kg at a power density of 184 W/kg, as presented in the Ragone plot (Fig. 7d). Several authors have previously reported symmetric supercapacitors based on Ni—C composites from biomass or waste (**Table S2**). However, the employed materials were externally doped with Ni salts to perform better, leading to metal contents over 15 % [54,55], several orders of magnitude greater than the presented materials. It is necessary to remember that in the present research, no external Ni has been added during pyrolysis apart from the adsorbed by the plants. In addition, the employed electrolyte is neutral, reducing the environmental impact of the device construction, in contrast to similar articles published in the past [54,56].

The stability of the device was assessed by 5000 GCD cycles (Fig. 8). The cell presented an excellent capacitance retention of almost 90 % and maintained the Coulombic efficiency near 100 %, as shown in **Fig. 8a** and **b**, respectively. The GCD transients (Fig. 8c) keep the triangular shape, although there exists a decrease in the capacitance and a slight

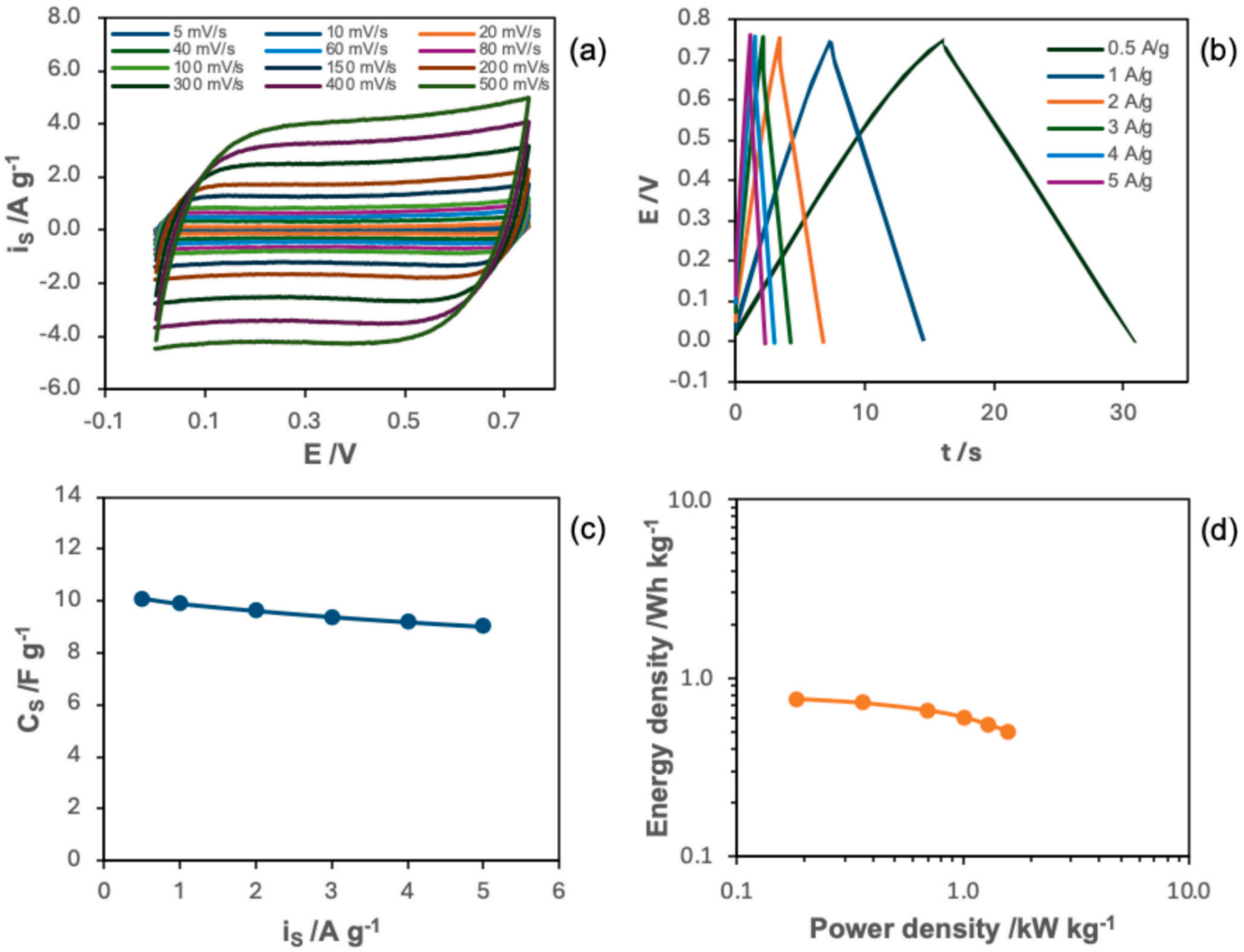

Fig. 7. Electrochemical performance of the symmetric cell made of sample D (1.6 g Ni/L): (a) Cyclic voltammograms at different scan rates (5, 10, 20, 40, 60, 80, 100, 150, 200, 300, 400 and 500 mV/s); (b) GCD at different applied currents (0.5, 1, 2, 3, 4 and 5 A/g); (c) Specific capacitance as a function of the applied current; (d) Ragone plot displaying the energy density as a function of the power density.

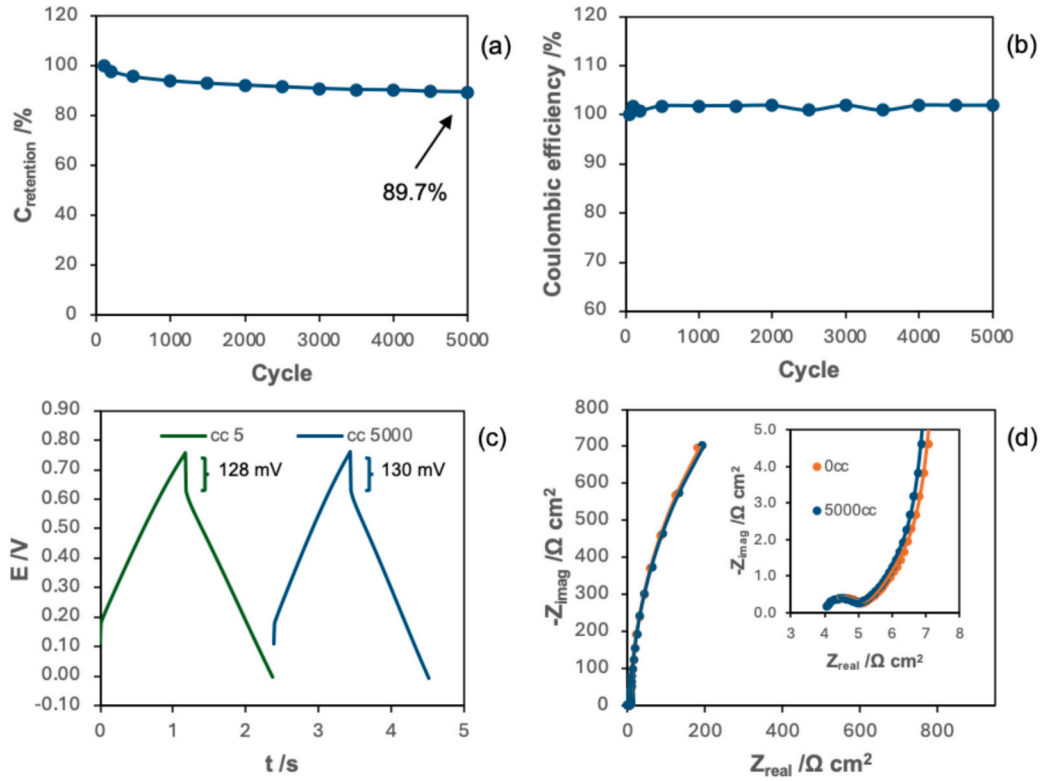

Fig. 8. Device stability characterisation in 1 M Na_2SO_4 for 5000 GCD cycles, at 5 A/g: (a) Capacitance retention; (b) Coulombic efficiency; (c) 5th and 5000th GCD cycles; (d) Nyquist plots before and after 5000 GCD cycles (dots – experimental data; line – fitted data).

increase in the ohmic drop of 2 mV after 5000 GCD cycles. Before and after GCD cycling, impedance spectra do not present a significant variation (Fig. 8d). The charge transfer resistance increased slightly after the long cycling (from 1.092 to 1.176 Ω cm^2), and the series resistance was 5 Ω cm^2.

Studying traditional nanocomposites is relatively straightforward due to their well-defined composition, but nanocomposites derived from plant biochar introduce complexity. As broccolis are cultivated with increasing Ni concentrations, N metabolism can be destabilised [31]. Chelating agents with high S content [38,39] can contribute to doping the carbon matrix alongside Ni nanoparticles (Fig. 4). However, several physiological changes occur; for example, increased ROS content

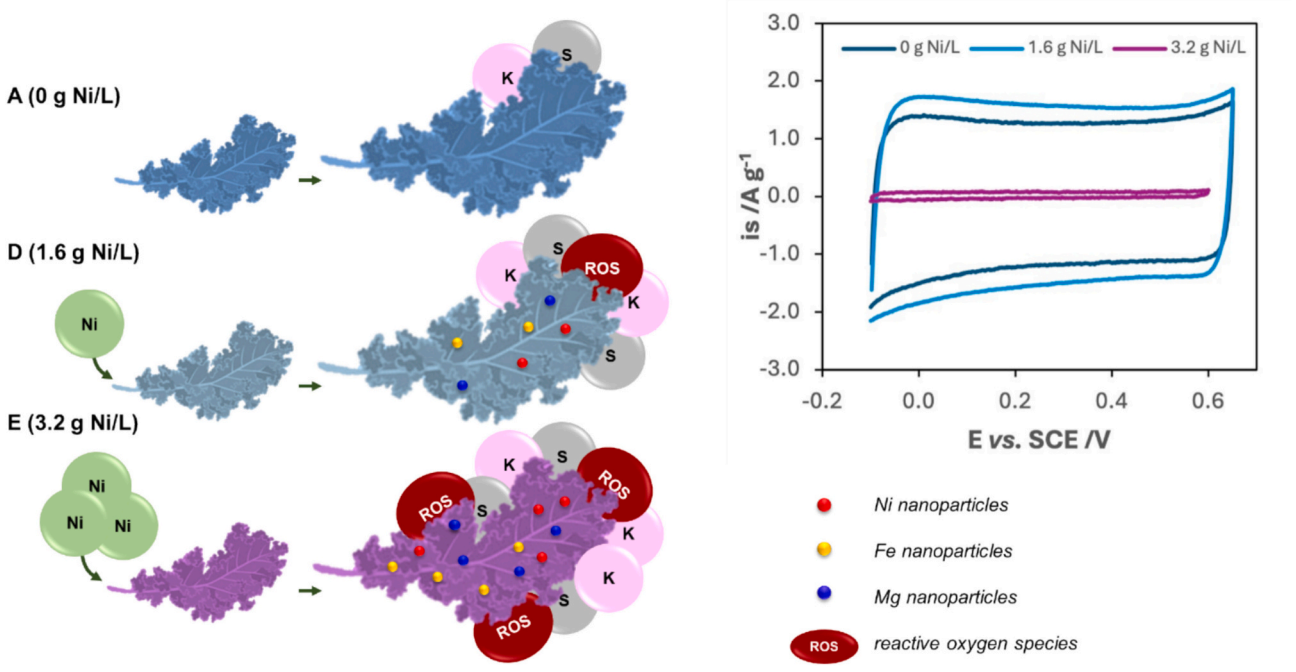

Fig. 9. Scheme of the proposed effect of Ni accumulation on broccoli and resulting electrochemical performance. The increased levels of reactive oxygen species (ROS) are supported by the literature [25,32,33], indicating that higher concentrations of Ni correlate with elevated ROS production.

[21,25,28,33] can compromise the quality of the carbon matrix. ROS, particularly hydroxyl radicals, interfere with plant metabolism by damaging carbohydrates, disrupting metabolic pathways such as the Calvin cycle, and fragmenting essential organic molecules [32]. Studies have also shown that ROS plays a role in cytoskeleton dynamics and cell expansion. Under heavy metal stress, ROS production increases, leading to further oxidative damage to plant structures, including cellulose and pectin [32]. Also, these systems exhibit homeostatic mechanisms to compensate for stressful conditions, leading to an increase in other electroactive and non-electroactive elements [21,25,28], further altering the final performance of the biochar. Therefore, the authors hypothesise that striking a delicate balance between increased Ni content and carbon doping while mitigating detrimental factors like ROS could ensure optimal electrochemical performance (Fig. 9). This aligns with current literature, demonstrating how oxidative stress impacts plant skeleton [32]. Further studies are needed to clarify the relationship between ROS management, Ni content, and biochar quality in electrochemical applications.

Overall, the accumulation of bioactive compounds in plants holds promise for engineering ecoconscious raw materials for energy storage applications, introducing enhanced metrics to address the predicted shortage amid increasing demand and promoting sustainability through environmental clearance. While promising, this strategy is still in its infancy, requiring concerted efforts from the scientific community to advance knowledge and mechanistic understanding.

4. Conclusions

Our findings provide novel insights into the potential of hyperaccumulators to offer ecoconscious materials for energy storage while simultaneously remedying environmental pollution caused by electroactive elements. Broccoli exposed to varying Ni concentrations (0, 0.4, 0.8, 1.6, and 3.2 g/L) over 10 weeks exhibited observable morphological changes in shoots, particularly affecting growth and leaf size with higher Ni concentrations, yet without significant differences in fresh or dry weight, suggesting inherent compensatory mechanisms within the plant. Pyrolysis of the resulting biomass at 650 °C revealed increasing porosity with increasing Ni content and formation of metallic Ni nanoparticles within the carbon matrix of broccoli-derived biochar, alongside Fe and Mg nanoparticles, as characterised by high-resolution transmission electron microscopy (HR-TEM) and X-ray diffraction (XRD) analyses. This incorporation of Ni into the carbon matrix enhanced the electrochemical performance of carbon-based materials, demonstrated by the suitability of broccoli biochar-derived electrodes for energy storage, where Ni content influences specific capacitance, capacitance retention and self-discharge. Surprisingly, optimal electrochemical performance was not observed in biomass with the highest Ni content but in those with 152 mg Ni/kg (or 1.6 g Ni/L). Notably, the resulting bionanocomposite exhibited a specific capacitance of 37.99 F/g at a high scan rate of 100 mV/s and excellent cyclic stability, retaining approximately 94 % of their capacitance after 5000 cycles at 10 A/g, highlighting their potential for long-term energy storage applications. As tested in a supercapacitor prototype, the device presented a maximum energy density of 0.762 Wh/kg at a power density of 184 W kg. These findings underscore the viability of engineering plant-derived biochar as ecoconscious and effective raw material for energy storage electrodes, providing a novel solution to bridge the gap in raw materials needed to meet the increasing demand for greener energy solutions. This emerging field offers numerous innovative solutions but raises many questions. To fully understand the role of Ni-loaded plant biochar in energy storage applications, the impact of various factors on Ni uptake, including soil pH, organic matter, competing ions, chelating agents, stressors (such as salinity and pathogenic attacks), and different plant species need to be investigated.

CRediT authorship contribution statement

Pablo Arévalo-Cid: Writing – review & editing, Validation, Methodology, Conceptualization. **Lorena Alcaraz:** Writing – review & editing, Validation, Methodology, Investigation. **R.S. Sampaio:** Writing – review & editing, Writing – original draft, Methodology. **Felix A. López-Gómez:** Writing – review & editing, Funding acquisition. **Patrícia A. Carvalho:** Writing – review & editing, Methodology, Conceptualization. **M.F. Montemor:** Writing – review & editing, Validation, Funding acquisition. **Marta M. Alves:** Writing – original draft, Validation, Methodology, Conceptualization.

Declaration of Generative AI and AI-assisted technologies in the writing process

During the preparation of this work, the author(s) used ChatGPT to correct and improve English writing. After using this tool, the author(s) reviewed and edited the content as needed and take(s) full responsibility for the publication's content.

Declaration of competing interest

The authors declare that they have no known competing financial interests or personal relationships that could have appeared to influence the work reported in this paper.

Acknowledgements

Authors thank the national funds from Fundação para a Ciência e a Tecnologia (FCT) in the scope of the Research Unit Centro de Química Estrutural (CQE) project UIDB/00100/2020 (https://doi.org/10.54499/UIDP/00100/2020) and UIDP/00100/2020 (https://doi.org/10.54499/UIDB/00100/2020), the Associate Laboratory Institute of Molecular Sciences (IMS) project LA/P/0056/2020 (https://doi.org/10.54499/LA/P/0056/2020), and the Research Council of Norway for financial support through the NORTEM Project No.197405.

Appendix A. Supplementary data

Supplementary data to this article can be found online at https://doi.org/10.1016/j.est.2025.115527.

Data availability

Data will be made available on request.

References

[1] M.Y.A. Khan, K.M. Gani, G.J. Chakrapani, Spatial and temporal variations of physicochemical and heavy metal pollution in Ramganga River—a tributary of river Ganges, India, Environ. Earth Sci. 76 (5) (2017) 231, https://doi.org/10.1007/s12665-017-6547-3.

[2] A. Kumar, D.K. Jigyasu, A. Kumar, G. Subrahmanyam, R. Mondal, A.A. Shabnam, M.M.S. Cabral-Pinto, S.K. Malyan, A.K. Chaturvedi, D.K. Gupta, R.K. Fagodiya, S. A. Khan, A. Bhatia, Nickel in terrestrial biota: comprehensive review on contamination, toxicity, tolerance and its remediation approaches, Chemosphere 275 (2021) 129996, https://doi.org/10.1016/j.chemosphere.2021.129996.

[3] S. Ding, D.-X. Guan, Z.-H. Dai, J. Su, H.H. Teng, J. Ji, Y. Liu, Z. Yang, L.Q. Ma, Nickel bioaccessibility in soils with high geochemical background and anthropogenic contamination, Environ. Pollut. 310 (2022) 119914, https://doi.org/10.1016/j.envpol.2022.119914.

[4] M.S.A. Ahmad, M. Ashraf, Essential roles and hazardous effects of nickel in plants, in: D.M. Whitacre (Ed.), Reviews of Environmental Contamination and Toxicology, Springer, New York, New York, NY, 2011, pp. 125–167, https://doi.org/10.1007/978-1-4614-0668-6_6.

[5] P. Gianniantonio, P. Francesca, R. Irene, Bioavailability and bioaccessibility in soil: a short review and a case study, AIMS Environmental Science 7 (2) (2020) 208–225, https://doi.org/10.3934/environsci.2020013.

[6] W. Xu, X. Zhao, F. Zhan, Q. He, H. Wang, J. Chen, H. Wang, X. Ren, L. Chen, Toward emerging two-dimensional nickel-based materials for electrochemical

energy storage: Progress and perspectives, Energy Storage Materials 53 (2022) 79–135, https://doi.org/10.1016/j.ensm.2022.08.039.
[7] P. Dilshara, B. Abeysinghe, R. Premasiri, N. Dushyantha, N. Ratnayake, S. Senarath, A. Sandaruwan Ratnayake, N. Batapola, The role of nickel (Ni) as a critical metal in clean energy transition: applications, global distribution and occurrences, production-demand and phytomining, J. Asian Earth Sci. 259 (2024) 105912, https://doi.org/10.1016/j.jseaes.2023.105912.
[8] P. Poizot, F. Dolhem, Clean energy new deal for a sustainable world: from non-CO2 generating energy sources to greener electrochemical storage devices, Energy Environ. Sci. 4 (6) (2011) 2003–2019, https://doi.org/10.1039/C0EE00731E.
[9] J. Robinson, N. Kumari, V.K. Srivastava, N. Taskaeva, C. Mohan, Sustainable and environmental friendly energy materials, Materials Today: Proceedings 69 (2022) 494–498, https://doi.org/10.1016/j.matpr.2022.09.187.
[10] A. Mustafa, U. Zulfiqar, M.Z. Mumtaz, M. Radziemska, F.U. Haider, J. Holatko, T. Hammershmiedt, M. Naveed, H. Ali, A. Kintl, Q. Saeed, J. Kucerik, M. Brtnicky, Nickel (Ni) phytotoxicity and detoxification mechanisms: a review, Chemosphere 328 (2023) 138574, https://doi.org/10.1016/j.chemosphere.2023.138574.
[11] M. Amjad, H. Raza, B. Murtaza, G. Abbas, M. Imran, M. Shahid, M.A. Naeem, A. Zakir, M.M. Iqbal, Nickel toxicity induced changes in nutrient dynamics and antioxidant profiling in two maize (*Zea mays* L.), Hybrids, Plants 9 (1) (2020) 5, https://doi.org/10.3390/plants9010005.
[12] L. Van der Pas, R.A. Ingle, Towards an understanding of the molecular basis of nickel Hyperaccumulation in plants, Plants 8 (1) (2019) 11, https://doi.org/10.3390/plants8010011.
[13] X. Chen, A. Chu, D. Li, Y. Yuan, X. Fan, Y. Deng, Development of the cycling life model of Ni-MH power batteries for hybrid electric vehicles based on real-world operating conditions, Journal of Energy Storage 34 (2021) 101999, https://doi.org/10.1016/j.est.2020.101999.
[14] Y. Jiang, C. Zhou, J. Liu, A non-polarity flexible asymmetric supercapacitor with nickel nanoparticle@ carbon nanotube three-dimensional network electrodes, Energy Storage Materials 11 (2018) 75–82, https://doi.org/10.1016/j.ensm.2017.09.013.
[15] X. Wu, H. Zhang, K.-J. Huang, Z. Chen, Stabilizing metallic Iron nanoparticles by conformal graphitic carbon coating for high-rate anode in Ni–Fe batteries, Nano Lett. 20 (3) (2020) 1700–1706, https://doi.org/10.1021/acs.nanolett.9b04867.
[16] G. Jiang, S. Osman, R.A. Senthil, Y. Sun, X. Tan, J. Pan, Hierarchically porous carbon derived from magnesium-based metal-organic frameworks as advanced active material for supercapacitor, Journal of Energy Storage 49 (2022) 104071, https://doi.org/10.1016/j.est.2022.104071.
[17] K.M. Shell, S.Y. Vohra, D.D. Rodene, R.B. Gupta, Phytoremediation of nickel via water hyacinth for biocarbon-derived supercapacitor applications, Energ. Technol. 9 (8) (2021) 2100130, https://doi.org/10.1002/ente.202100130.
[18] V. Hoffmann, C. Rodriguez Correa, D. Sautter, E. Maringolo, A. Kruse, Study of the electrical conductivity of biobased carbonaceous powder materials under moderate pressure for the application as electrode materials in energy storage technologies, GCB Bioenergy 11 (1) (2019) 230–248, https://doi.org/10.1111/gcbb.12545.
[19] Z. Chen, M. Zhang, Y. Wang, Z. Yang, D. Hu, Y. Tang, K. Yan, Controllable synthesis of nitrogen-doped porous carbon from metal-polluted miscanthus waste boosting for supercapacitors, Green Energy & Environment 6 (6) (2021) 929–937, https://doi.org/10.1016/j.gee.2020.07.015.
[20] T. Jiang, Y. Zhang, S. Olayiwola, C. Lau, M. Fan, K. Ng, G. Tan, Biomass-derived porous carbons support in phase change materials for building energy efficiency: a review, Materials Today Energy 23 (2022) 100905, https://doi.org/10.1016/j.mtener.2021.100905.
[21] M. Natasha, M. Shahid, H. Saleem, S. Anwar, T.Z. Khalid, B. Tariq, M. Murtaza, M. A. Amjad, Naeem, a multivariate analysis of comparative effects of heavy metals on cellular biomarkers of phytoremediation using *Brassica oleracea*, Int. J. Phytoremediation 22 (6) (2020) 617–627, https://doi.org/10.1080/15226514.2019.1701980.
[22] M.U. Hassan, M.U. Chattha, I. Khan, M.B. Chattha, M. Aamer, M. Nawaz, A. Ali, M. A.U. Khan, T.A. Khan, Nickel toxicity in plants: reasons, toxic effects, tolerance mechanisms, and remediation possibilities—a review, Environ. Sci. Pollut. Res. 26 (13) (2019) 12673–12688, https://doi.org/10.1007/s11356-019-04892-x.
[23] I.V. Drozdova, N.V. Alekseeva-Popova, I.B. Kalimova, A.I. Belyaeva, N. A. Smirnova, The accumulating ability and nickel tolerance of Brassicaceae species of the North Caucasus in connection with the problem of phytoremediation, J. Geochem. Explor. 182 (2017) 235–241, https://doi.org/10.1016/j.gexplo.2017.03.001.
[24] M.N. Cempel, G. Nickel, a review of its sources and environmental toxicology, Pol. J. Environ. Stud. 15 (3) (2006) 375–382.
[25] B. Shahzad, M. Tanveer, A. Rehman, S.A. Cheema, S. Fahad, S. Rehman, A. Sharma, Nickel; whether toxic or essential for plants and environment - a review, Plant Physiol. Biochem. 132 (2018) 641–651, https://doi.org/10.1016/j.plaphy.2018.10.014.
[26] S. Lopez, A. van der Ent, P.D. Erskine, G. Echevarria, J.L. Morel, G. Lee, E. Permana, E. Benizri, Rhizosphere chemistry and above-ground elemental fractionation of nickel hyperaccumulator species from Weda bay (Indonesia), Plant Soil 436 (1) (2019) 543–563, https://doi.org/10.1007/s11104-019-03954-w.
[27] J. Molas, Changes in morphological and anatomical structure of cabbage (*Brassica oleracea* L.) outer leaves and in ultrastructure of their chloroplasts caused by an in vitro excess of nickel, Photosynthetica 34 (4) (1998) 513–522, https://doi.org/10.1023/A:1006805327340.
[28] C. Chen, D. Huang, J. Liu, Functions and toxicity of nickel in plants: recent advances and future prospects, CLEAN – soil, Air, Water 37 (4–5) (2009) 304–313, https://doi.org/10.1002/clen.200800199.
[29] L. Kong, M. Zhong, W. Shuang, Y. Xu, X.-H. Bu, Electrochemically active sites inside crystalline porous materials for energy storage and conversion, Chem. Soc. Rev. 49 (8) (2020) 2378–2407, https://doi.org/10.1039/C9CS00880B.
[30] M. Karatassiou, A. Giannakoula, D. Tsitos, S. Stefanou, Response of three Greek populations of *Aegilops triuncialis* (crop wild relative) to serpentine soil, Plants 10 (3) (2021) 516, https://doi.org/10.3390/plants10030516.
[31] C.-P. Witte, Urea metabolism in plants, Plant Sci. 180 (3) (2011) 431–438, https://doi.org/10.1016/j.plantsci.2010.11.010.
[32] R. Schmidt, A.B. Kunkowska, J.H.M. Schippers, Role of reactive oxygen species during cell expansion in leaves, Plant Physiol. 172 (4) (2016) 2098–2106, https://doi.org/10.1104/pp.16.00426.
[33] A. Zaid, F. Mohammad, S.H. Wani, K.M.H. Siddique, Salicylic acid enhances nickel stress tolerance by up-regulating antioxidant defense and glyoxalase systems in mustard plants, Ecotoxicol. Environ. Saf. 180 (2019) 575–587, https://doi.org/10.1016/j.ecoenv.2019.05.042.
[34] G. Yang, C. Pan, H. Yang, N. Feng, Carbon-supported nickel catalyst prepared from steam-exploded poplar by recovering Ni(II), BioResources 16 (3) (2021) 5481–5493, https://doi.org/10.15376/biores.16.3.5481-5493.
[35] W. Wang, C. Duong-Viet, L. Truong-Phuoc, J.-M. Nhut, L. Vidal, C. Pham-Huu, Activated carbon supported nickel catalyst for selective CO2 hydrogenation to synthetic methane under contactless induction heating, Catal. Today 418 (2023) 114073, https://doi.org/10.1016/j.cattod.2023.114073.
[36] A. Adan-Mas, L. Alcaraz, P. Arévalo-Cid, F.A. López-Gómez, F. Montemor, Coffee-derived activated carbon from second biowaste for supercapacitor applications, Waste Manag. 120 (2021) 280–289, https://doi.org/10.1016/j.wasman.2020.11.043.
[37] A.R. Selvaraj, D. Chinnadurai, I. Cho, J.-S. Bak, K. Prabakar, Bio-waste wood-derived porous activated carbon with tuned microporosity for high performance supercapacitors, Journal of Energy Storage 52 (2022) 104928, https://doi.org/10.1016/j.est.2022.104928.
[38] O. Sytar, S. Ghosh, H. Malinska, M. Zivcak, M. Brestic, Physiological and molecular mechanisms of metal accumulation in hyperaccumulator plants, Physiol. Plant. 173 (1) (2021) 148–166, https://doi.org/10.1111/ppl.13285.
[39] J.L. Freeman, M.W. Persans, K. Nieman, C. Albrecht, W. Peer, I.J. Pickering, D. E. Salt, Increased glutathione biosynthesis plays a role in nickel tolerance in Thlaspi nickel Hyperaccumulators, Plant Cell 16 (8) (2004) 2176–2191, https://doi.org/10.1105/tpc.104.023036.
[40] M. Guilpain, B. Laubie, X. Zhang, J.L. Morel, M.-O. Simonnot, Speciation of nickel extracted from hyperaccumulator plants by water leaching, Hydrometallurgy 180 (2018) 192–200, https://doi.org/10.1016/j.hydromet.2018.07.024.
[41] A.L.D. Paul, V. Gei, S. Isnard, B. Fogliani, G. Echevarria, P.D. Erskine, T. Jaffré, J. Munzinger, A. van der Ent, Nickel hyperaccumulation in new Caledonian Hybanthus (Violaceae) and occurrence of nickel-rich phloem in Hybanthus austrocaledonicus, Ann. Bot. 126 (5) (2020) 905–914, https://doi.org/10.1093/aob/mcaa112.
[42] M. Ater, C. Lefèbvre, W. Gruber, P. Meerts, A phytogeochemical survey of the flora of ultramafic and adjacent normal soils in North Morocco, Plant Soil 218 (1) (2000) 127–135, https://doi.org/10.1023/A:1014925007960.
[43] M. Waqas, A.S. Aburiazaiza, R. Miandad, M. Rehan, M.A. Barakat, A.S. Nizami, Development of biochar as fuel and catalyst in energy recovery technologies, J. Clean. Prod. 188 (2018) 477–488, https://doi.org/10.1016/j.jclepro.2018.04.017.
[44] H. Wang, X. Kou, J. Zhang, J. Li, Large scale synthesis and characterization of Ni nanoparticles by solution reduction method, Bull. Mater. Sci. 31 (1) (2008) 97–100, https://doi.org/10.1007/s12034-008-0017-1.
[45] T.-H.-B. Deng, A. van der Ent, Y.-T. Tang, T. Sterckeman, G. Echevarria, J.-L. Morel, R.-L. Qiu, Nickel hyperaccumulation mechanisms: a review on the current state of knowledge, Plant Soil 423 (1) (2018) 1–11, https://doi.org/10.1007/s11104-017-3539-8.
[46] P. Arévalo-Cid, M.F. Vaz, M.F. Montemor, Highly porous FeNi 3D foams produced by one-step electrodeposition: electrochemical stability and mechanical properties, Mater. Charact. 193 (2022) 112311, https://doi.org/10.1016/j.matchar.2022.112311.
[47] Z. Bai, H. Chen, B. Li, W. Li, Methane decomposition over Ni loaded activated carbon for hydrogen production and the formation of filamentous carbon, Int. J. Hydrog. Energy 32 (1) (2007) 32–37, https://doi.org/10.1016/j.ijhydene.2006.06.030.
[48] J. Cebollada, D. Sebastián, M.J. Lázaro, M.V. Martínez-Huerta, Carbonized Polydopamine-based nanocomposites: the effect of transition metals on the oxygen Electrocatalytic activity, Nanomaterials 13 (9) (2023) 1549, https://doi.org/10.3390/nano13091549.
[49] L. Ji, Z. Lin, M. Alcoutlabi, O. Toprakci, Y. Yao, G. Xu, S. Li, X. Zhang, Electrospun carbon nanofibers decorated with various amounts of electrochemically-inert nickel nanoparticles for use as high-performance energy storage materials, RSC Adv. 2 (1) (2012) 192–198, https://doi.org/10.1039/C1RA00676B.
[50] P. Navalpotro, M. Anderson, R. Marcilla, J. Palma, Insights into the energy storage mechanism of hybrid supercapacitors with redox electrolytes by electrochemical impedance spectroscopy, Electrochim. Acta 263 (2018) 110–117, https://doi.org/10.1016/j.electacta.2017.12.167.
[51] G.J. Brug, A.L.G. van den Eeden, M. Sluyters-Rehbach, J.H. Sluyters, The analysis of electrode impedances complicated by the presence of a constant phase element, J. Electroanal. Chem. Interfacial Electrochem. 176 (1) (1984) 275–295, https://doi.org/10.1016/S0022-0728(84)80324-1.
[52] Y. Wang, Y. Zhang, L. Pei, D. Ying, X. Xu, L. Zhao, J. Jia, X. Cao, Converting Ni-loaded biochars into supercapacitors: implication on the reuse of exhausted

carbonaceous sorbents, Sci. Rep. 7 (1) (2017) 41523, https://doi.org/10.1038/srep41523.

[53] S. Ardizzone, G. Fregonara, S. Trasatti, "Inner" and "outer" active surface of RuO_2 electrodes, Electrochim. Acta 35 (1) (1990) 263–267, https://doi.org/10.1016/0013-4686(90)85068-X.

[54] S. Zhang, Y. Pang, Y. Wang, B. Dong, S. Lu, M. Li, S. Ding, NiO nanosheets anchored on honeycomb porous carbon derived from wheat husk for symmetric supercapacitor with high performance, J. Alloys Compd. 735 (2018) 1722–1729, https://doi.org/10.1016/j.jallcom.2017.11.294.

[55] A. Pradiprao Khedulkar, V. Dien Dang, B. Pandit, T. Ai Ngoc Bui, H. Linh Tran, R.-a. Doong, Flower-like nickel hydroxide@tea leaf-derived biochar composite for high-performance supercapacitor application, J. Colloid Interface Sci. 623 (2022) 845–855. doi:https://doi.org/10.1016/j.jcis.2022.04.178.

[56] R.-X. Xu, Y.-P. Zhao, G.-H. Liu, J.-S. Zhu, R.-Y. Wang, J.-P. Cao, X.-Y. Wei, N/O co-doped porous interconnected carbon nanosheets from the co-hydrothermal treatment of soybean stalk and nickel nitrate for high-performance supercapacitors, J. Colloid Interface Sci. 558 (2020) 211–219, https://doi.org/10.1016/j.jcis.2019.09.097.